

Weighing the Axion with Muon Haloscopy

N. Bray-Ali ^{a,1}

^a *Science Synergy,
Los Angeles, CA 90045, USA*

E-mail: nbrayali@gmail.com

ABSTRACT: Recent measurements of muon spin precession confirm a long-standing tension with the Standard Model of particle physics. We argue that axions from the local dark matter halo of the galaxy are responsible for the tension. The argument yields a percent level prediction for the mass of the axion provided that dark matter is made of axions. An analysis of charge asymmetry in kaon decays suggests that at least in the local halo dark matter is made of axions and that axions from the local halo are responsible for the observed violation by these reactions of the combined charge conjugation and spatial inversion symmetry operation. Tabletop experiments to directly detect dark matter in the form of axions with the predicted mass are proposed.

¹Corresponding author.

Contents

1	Introduction	1
2	Nature of Dark Matter	2
3	Kaon Haloscopy	2
4	Muon Haloscopy	3
5	Proton Haloscopy	4
6	Atomic Haloscopy	5
7	Cyclotron Haloscopy	6
8	Microwave Haloscopy	6
9	Bend Magnet Haloscopy	7
10	Electromagnon Haloscopy	8
11	Conclusion	9

1 Introduction

The spin of the muon precesses in a magnetic field B at frequency $\omega_a = a_\mu(e/m_\mu)B$, where, $a_\mu \approx \alpha/(2\pi) \approx 1.16 \times 10^{-3}$ is the electromagnetic leading order contribution to spin precession, and $e/m_\mu = 2\pi \times 135 \text{ MHz/T}$ is the charge to mass ratio of the muon [1-4]. Compared with the electron, the muon is $(m_\mu/m_e)^2 \approx 43,000$ times more sensitive to the hadronic leading order contribution $a_\mu^{\text{HLO}} \approx 700 \times 10^{-10}$ to spin precession [5, 6]. In this Article, we show that axions in the local dark matter halo of the galaxy shift a_μ and a_μ^{HLO} from their standard model values. Further, we argue that the size of these axion-induced shifts explains the tension between measurements of the muon spin precession frequency [2, 3] and calculations of the frequency based on measurements of the hadronic leading order contribution [5] provided that dark matter in the local halo is made of axions as suggested by analysis of charge asymmetry between the kaon decay $K_L^0 \rightarrow \pi^+ e^- \bar{\nu}_e$ and its charge-parity conjugate $K_L^0 \rightarrow \pi^- e^+ \nu_e$ [7-11]. Finally, we give a physical picture for the nature of dark matter that leads to a prediction for the mass of the axion with percent level precision and we sketch table-top experiments for testing this prediction.

2 Nature of Dark Matter

We start by expressing the axion A_M in terms of quarks and leptons M_H^P with helicity $H = L, R$ and charge-parity check $P = +, -$ [13]:

$$A_M = M_L^- \overline{M}_R^- - M_R^- \overline{M}_L^- - M_L^+ \overline{M}_R^+ + M_R^+ \overline{M}_L^+ \quad (2.1)$$

Here, M runs over the twelve known “flavors” of quarks and leptons while the charge-parity check P is $+$ for quarks and leptons that do not feel the weak nuclear force and $-$ for those that do. In the standard model, we find M_L^- and M_R^+ , but neither M_L^+ nor M_R^- , where, L is for left-handed and R is for right-handed helicity [14].

Next, we suppose that axions A_M of each kind and photons γ_H of each helicity formed in equal numbers in the early universe prior to baryogenesis. This fixes the ratio $n_A/n_\gamma = |M|/|H| = 6$ of axions to photons and gives the axion mass m_A ($\hbar = c = 1$) [15]:

$$m_A = 2.70 kT_\gamma \left(\frac{n_A}{n_\gamma} \right)^{-1} \frac{\Omega_A h^2}{\Omega_\gamma h^2} = (0.508 \pm 0.004) \text{ eV}, \quad (2.2)$$

where, $T_\gamma = (2.7255 \pm 0.0006)$ K is the present photon temperature [16], $\Omega_\gamma h^2 = 2.473 \times 10^{-5}$ is the photon energy density parameter and $\Omega_A h^2 = 0.11882 \pm 0.00086$ is that of the axions assuming dark matter is made of axions [17].

3 Kaon Haloscopy

The energy density of axions in the local dark matter halo of the galaxy ρ_A can be estimated using the charge asymmetry of kaon decays [18]:

$$A_L(e) = -2\sqrt{2}\xi_{A\pi} p_K \tilde{\phi}_A(q_A) = 4\pi C_{A\pi} \frac{f_\pi \sqrt{\rho_A h c}}{m_A f_A} L_K, \quad (3.1)$$

where, the axion amplitude $\tilde{\phi}_A(q_A)$ at momentum q_A changes sign under the combination of charge conjugation and space inversion probed by $A_L(e)$ to create the observed charge asymmetry [13]. The mixing angle $\xi_{A\pi} = -C_{A\pi} f_\pi / f_A$ between the axion A and the neutral pion π^0 can be expressed in terms of the pion decay constant $f_\pi = (92.32 \pm 0.09)$ MeV [19], the axion decay constant f_A [20], and the light quark masses using $C_{A\pi} = (m_d - m_u)/(2m_u + 2m_d) = (0.173 \pm 0.08)$ [21]. Here, the kaon beam has momentum p_K and decays in-flight within a detector of length L_K .

Meanwhile, the axion mass m_A and the decay constant f_A only enter the kaon charge asymmetry through the product $m_A f_A = \sqrt{\chi_{\text{QCD}}} = (5.69 \pm 0.05) \times 10^{-3}$ GeV 2 which is fixed by the topological susceptibility χ_{QCD} of the quantum chromodynamic vacuum [22]. Using the kaon parameters $L_K = 500$ cm and $A_L(e) = (3.32 \pm 0.08) \times 10^{-3}$ from the current best charge asymmetry measurement [12], the local axion energy density $\rho_A = (0.28 \pm 0.03)$ GeV/cm 3 that we find from Eq. (3.1) agrees with the best available estimate $\rho_{\text{DM}} = (0.30 \pm 0.03)$ GeV/cm 3 of the energy density of the local dark matter halo [23]. This agreement suggests that axions saturate the local dark matter halo and that dark matter from the local halo is the source of the charge asymmetry observed in kaon decays [24].

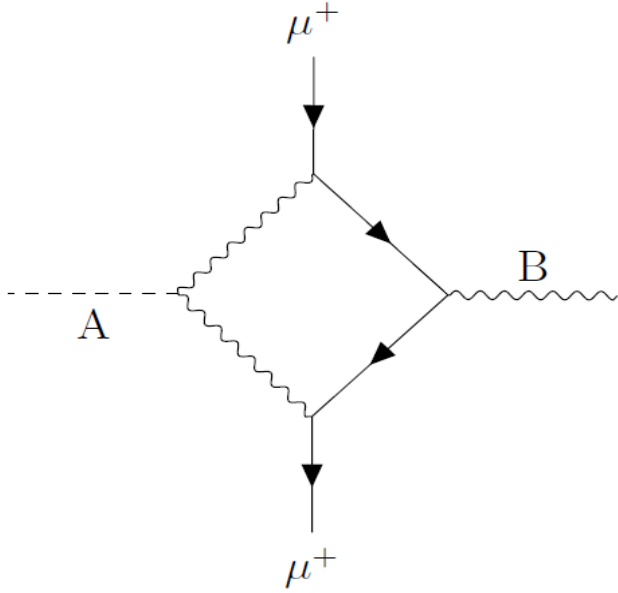


Figure 1. Halo axion A collides with virtual photon or vector meson dressing vertex of positive muon μ^+ and magnetic field B .

4 Muon Haloscopy

Figure 1 shows how axions in the local dark matter halo shift muon spin precession [2–4]. Acting as a background field $\tilde{\phi}_A(q_A)$ with on-shell four-momentum $q_A^2 = m_A^2 \ll m_\mu^2$, the axion A couples to the virtual photon dressing the vertex of the positive muon μ^+ and the magnetic field B . The shift of the spin precession frequency Δa_μ goes as the strength of the coupling $g_{A\gamma\gamma}$ between the axion and a pair of photons [25]:

$$\frac{\Delta a_\mu}{a_\mu} = m_A^2 g_{A\gamma\gamma} \tilde{\phi}_A(q_A) = \pm m_A g_{A\gamma\gamma} \sqrt{\rho_A N_\mu V_\mu T_\mu} \quad (4.1)$$

where, the axion field strength $|\tilde{\phi}_A(q_A)|^2 \approx \phi_A^2 N_\mu V_\mu T_\mu$ is fixed by the axion energy density $\rho_A = \phi_A^2 m_A^2$, the volume V_μ of the muon beam, the lifetime T_μ of the muon in the axion rest-frame, and the average number of muons N_μ during spin precession. The sign of the shift Δa_μ in Eq. (4.1) switches along with the axion field $\tilde{\phi}_A(q_A)$ under spatial inversion P , under time-reversal T , and under the combinations CP and CT with charge conjugation C [26]. The size of the shift scales up with square root of the effective four-volume $\sqrt{N_\mu V_\mu T_\mu}$ of the muon beam.

The shift in the muon spin precession frequency Δa_μ due to axions in the local dark matter halo of the galaxy has roughly the right size to resolve the tension $a_\mu(\text{Exp}) - a_\mu(\text{SM}) = (251 \pm 59) \times 10^{-11}$ between experiments (Exp) [2, 3] and standard model calculations (SM) [5, 6]. The axion-photon coupling strength is $g_{A\gamma\gamma} = (0.68 \pm 0.02) \times 10^{-10} \text{ GeV}^{-1}$ for the axion mass $m_A = (0.508 \pm 0.004) \text{ eV}$ [27]. Combining these inputs, we find that the shift $\Delta a_\mu = (163 \pm 10) \times 10^{-11}$ of the muon spin precession frequency due to axions in the

local dark matter halo roughly resolves the tension between experiment and the standard model [28].

Figure 1 also shows how axions from the local dark matter halo of the galaxy shift measurements of the leading order hadronic contribution a_μ^{HLO} to muon spin precession [4, 5]. The axions collide with the ρ^0 vector meson that dominates the hadronic production from electron-positron annihilation whose cross-section enters the standard model calculation of a_μ^{HLO} . The collisions convert the short-lived ρ^0 meson, which produces mainly charged pion $\pi^+\pi^-$ pairs, into the longer lived and slightly heavier ω meson, which prefers to produce a neutral pion π^0 in addition to the charged pion pair. The conversions reduce the $\pi^+\pi^-$ hadronic production cross-section at the ρ^0 resonance and shift the calculated value of the leading order hadronic contribution by an amount set by the coupling $g_{A\rho\omega}$ of the axion to the ρ^0 and ω vector mesons [29]:

$$\begin{aligned} \frac{\Delta a_\mu^{\text{HLO}}}{a_\mu^{\text{HLO}}} &= m_A p_\rho g_{A\rho\omega} \tilde{\phi}_A(q_A) \\ &= \frac{\alpha}{3} \frac{\Delta a_\mu}{a_\mu} \frac{p_\rho}{m_A} \sqrt{\frac{m_\rho}{\Gamma_\rho^{ee}} \frac{m_\omega}{\Gamma_\omega^{ee}} \frac{1}{N_\mu} \frac{V_\rho}{V_\mu} \frac{T_\rho}{T_\mu}}, \end{aligned} \quad (4.2)$$

where, the mass of the vector meson $V = \rho, \omega$ is m_V , the partial width Γ_V^{ee} gives the rate that V produces an electron-positron pair, V_ρ is the luminous volume created by the colliding electron and positron bunches, T_ρ is the time it takes the bunches to cross during the collision, and p_ρ is the momentum of the ρ^0 vector meson in the axion rest frame. The shift $\Delta a_\mu^{\text{HLO}}$ in the hadronic contribution combines with the shift Δa_μ in the spin precession frequency to give a gap between experiment and the standard model $\Delta a_\mu + \Delta a_\mu^{\text{HLO}} = (311 \pm 18) \times 10^{-11}$ that is quite close to the observed tension [30].

5 Proton Haloscopy

Inverting the process shown in Figure 1 about a horizontal axis and replacing the muon with a proton, we find the way that axions from the local dark matter halo of the galaxy shift the spin precession of protons in the molecules of a liquid during nuclear magnetic resonance [31]:

$$\Delta g'_p = \frac{\alpha}{\pi\epsilon} m_A^2 g_{A\gamma\gamma} \tilde{\phi}_A(q_A) = 2 \frac{\Delta a_\mu}{\epsilon} \sqrt{\frac{N_p}{N_\mu} \frac{V_p}{V_\mu} \frac{T_p}{T_\mu}}, \quad (5.1)$$

where, ϵ is the static dielectric constant of the liquid and $g'_p \approx 5.58$ gives the proton spin precession frequency $\omega'_p = (g'_p/2)(e/m_p)B \approx 2\pi \times 42.8 \text{ MHz}/\text{T} \times B$ for magnetic field B [32]. Here, N_p is the effective number of protons, V_p is the volume containing the protons, and $T_p = 1/\Delta\omega'_p$ is the effective coherence time of the proton spin precession due to the broadening $\Delta\omega'_p$ of the resonance by variations in the field strength over the sample volume. Straightforward estimates of the proton parameters give the slope of the axion shift of the proton spin precession frequency [33]

$$\frac{1}{g'_p} \frac{dg'_p}{dT} = -(10.0 \pm 0.6) \text{ ppb/K} \left(\frac{\epsilon}{78.4} \right)^{-1} \left(\frac{V_p}{0.62 \text{ cm}^3} \right) \left(\frac{\Delta\omega'_p}{2.6 \times 10^{-7} \omega'_p} \right)^{-1/2}, \quad (5.2)$$

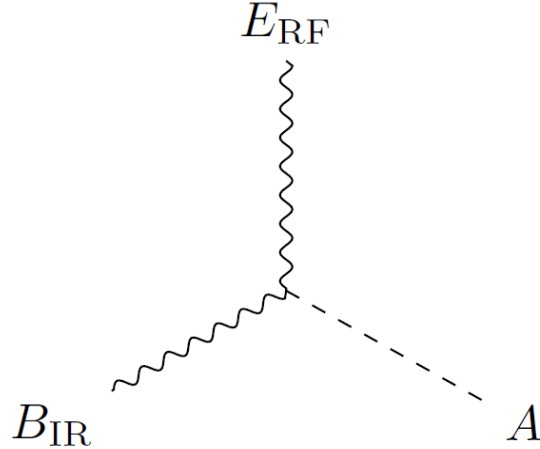


Figure 2. Dark matter A from the local halo of the galaxy converts infrared magnetic field B_{IR} into radio-frequency electric field E_{RF} that drives electron cyclotron motion and microwave cavity resonance.

where, $T \approx 300$ K is the temperature. Measurements of proton spin precession in liquids with the necessary precision to see the dark matter shift were achieved half a century ago [32]. Verifying the proton parameter dependence shown in Eq. (5.2) of the slope dg'_p/dT would directly confirm in a tabletop experiment the proposed mechanism for the shift of spin precession by axions from the local dark matter halo with the predicted mass.

6 Atomic Haloscopy

Replacing the positive muon in Figure 1 with the valence electron of an atom with large atomic number trapped in an optical lattice and replacing the external magnetic field with the internal magnetic field within the atom [34], we find the process that shifts the electromagnetic fine-structure coupling constant α felt by the electron during transitions among valence states:

$$\frac{\Delta\alpha}{\alpha} = m_A^2 g_{A\gamma\gamma} \tilde{\phi}_A(q_A) = \frac{\Delta a_\mu}{a_\mu} \sqrt{\frac{N_a}{N_\mu} \frac{V_a}{V_\mu} \frac{T_a}{T_\mu}}, \quad (6.1)$$

where, N_a is the number of atoms trapped in the optical lattice, V_a is the trap volume, and T_a is the coherence time for the motion of the ultracold atoms. The shift in α leads to a density-shift of the optical lattice clock frequency [35]:

$$\begin{aligned} \frac{\Delta\nu}{\nu} &= k_\alpha \frac{\Delta\alpha}{\alpha} \\ &= (11.8 \pm 0.7) \times 10^{-17} \left(\frac{N_a}{100} \right)^{1/2} \left(\frac{V_0}{200 E_R} \right)^{-3/4} \left(\frac{T}{9 \mu\text{K}} \right)^{1/4} \\ &\quad \times \left(\frac{k_\alpha}{0.24} \right) \left(\frac{E_R}{h \times 2.0 \text{ kHz}} \right)^{-3/2} \left(\frac{m}{171 m_p} \right)^{-3/4} \left(\frac{w}{26.4 \lambda_L} \right) \end{aligned} \quad (6.2)$$

where, k_α is the sensitivity of the transition frequency to shifts in the fine-structure constant, $E_R = h^2/(2m\lambda_L^2)$ is the kinetic energy with which the atoms of mass m recoil when they spontaneously emit photons at the wavelength λ_L of the optical lattice, V_0 is the lattice depth, w is the lattice laser beam waist, and T is the temperature of the atoms in the trap. By modulating the number of atoms in the trap, the density shift of the optical lattice clock frequency due to the effect of dark matter on the fine-structure constant described by Eq. (6.2) can be observed [36].

7 Cyclotron Haloscopy

Figure 2 shows how dark matter drives electron cyclotron motion by converting infrared laser photons near the Compton wavelength $\lambda_A = 2\pi/m_A = (2441 \pm 19)$ nm into radio-frequency electromagnetic waves within a magnetically confined plasma. When the beat note between the infrared light and the Compton wavelength of dark matter hits the electron cyclotron resonance frequency $\omega_c = (e/m_e)B = 2\pi \times 28$ GHz ($B/1$ T) for the magnetic field of strength B that confines the plasma, the radio-frequency electric field created by the interference heats the electrons at the rate [37]

$$P_{\text{RF}} = \frac{1}{2} P_{\text{IR}} m_A^4 g_A^2 |\tilde{\phi}_A(q_A)|^2 = \frac{1}{2} P_{\text{IR}} \left(\frac{\Delta a_\mu}{a_\mu} \right)^2 \frac{n_e V_e}{N_\mu} \frac{V_e}{V_\mu} \frac{T_e}{T_\mu} \quad (7.1)$$

where, P_{IR} is the infrared power sent into the plasma, n_e is the density of plasma electrons, V_e is the volume of the infrared beam within the plasma, and T_e is set by the coherence time of the infrared light. The resonant heating of the plasma leads to a drop in the transmitted infrared power [38]

$$\frac{\Delta P_{\text{IR}}}{P_{\text{IR}}} = (6.5 \pm 0.8)\% \left(\frac{\Delta \nu_{\text{IR}}}{1 \text{ MHz}} \right)^{-1} \left(\frac{\beta}{0.8} \right) \left(\frac{T}{12,000 \text{ K}} \right)^{-1} \left(\frac{L}{100 \text{ cm}} \right)^2 \left(\frac{B}{0.32 \text{ T}} \right)^{-2} \quad (7.2)$$

where, $\Delta \nu_{\text{IR}}$ is the coherent line-width of the infrared laser, β is the ratio of the electron pressure to the magnetic energy density in the plasma, T is the temperature of the plasma, and L is the laser path length through the plasma. By monitoring the change in infrared transmission, the location of the resonance can be found and the mass of the dark matter can be measured for typical laser [39] and plasma parameters [40].

8 Microwave Haloscopy

Figure 2 also shows how the infrared magnetic field B_{IR} of laser photons passing through a microwave cavity converts under the influence of axions from the local dark matter halo of the galaxy into the radio-frequency electric field E_{RF} that excites the cavity to resonate with power [37]

$$P_{\text{RF}} = \frac{1}{2} P_{\text{IR}} \left(\frac{\Delta a_\mu}{a_\mu} \right)^2 \frac{1}{N_\mu} \frac{V_{\text{IR}}}{V_\mu} \frac{T_{\text{IR}}}{T_\mu}, \quad (8.1)$$

where, P_{IR} is the infrared laser power, V_{IR} is the volume of the infrared laser beam within the microwave cavity, and T_{IR} is the coherence time of the infrared laser. For a receiver

at noise temperature T_S and a search that takes total time T_A , the radio-frequency power gives resonant signal-to-noise ratio [41]

$$\text{SNR} = (10.0 \pm 1.2) \left(\frac{P_{\text{IR}}}{3 \text{ mW}} \right) \left(\frac{\Delta\nu_{\text{IR}}}{1 \text{ MHz}} \right)^{-1} \left(\frac{D}{1 \text{ cm}} \right)^2 \times \left(\frac{T_A}{10^6 \text{ sec}} \right)^{1/2} \left(\frac{L}{112 \text{ cm}} \right) \left(\frac{T_S}{77 \text{ K}} \right)^{-1}, \quad (8.2)$$

where, $\Delta\nu_{\text{IR}} = 1/(2\pi T_{\text{IR}})$ is the infrared laser line-width, D is the beam diameter, and L is the length of the cavity. For typical laser [39] and cavity [42] parameters, the mass of the axion can be determined with precision $h\Delta\nu_{\text{IR}}/(m_A c^2) = 8.2 \text{ ppb}$ that is more than double that of the mass of the muon $\Delta m_\mu/m_\mu = 22 \text{ ppb}$ [7] in a search time $T_A = 10^6 \text{ sec} \approx 12 \text{ days}$ that takes less than a month.

9 Bend Magnet Haloscopy

Replacing the infrared magnetic field in Figure 2 with the static magnetic field B_{DC} of a dipole bend magnet and swapping the radio-frequency electric field for an infrared electric field E_{IR} , we find the process for converting axions from the local dark matter halo of the galaxy into photons with infrared power [43]

$$P_{\text{IR}} = S_{\text{IR}} \left(\frac{B_{\text{DC}}^2 c^2}{2Z_0} \right) \left(\frac{\Delta a_\mu}{a_\mu} \right)^2 \frac{1}{N_\mu} \frac{V_{\text{IR}}}{V_\mu} \frac{T_{\text{IR}}}{T_\mu}, \quad (9.1)$$

where, S_{IR} is the photosensitive area of the infrared detector, V_{IR} is the volume of the resonant cavity formed by placing infrared mirrors at the entrance and exit of the bend magnet, and $T_{\text{IR}} = 1/(2\pi\Delta\nu_{\text{IR}})$ is the coherence time of the infrared laser with line-width $\Delta\nu_{\text{IR}}$ that is used to tune the cavity to the resonance frequency $\omega_A = m_A c^2/\hbar = 2\pi \times (122.7 \pm 1.0) \text{ THz}$ set by the rest-mass of dark matter. Scanning the infrared frequency through this window of width $\Delta\omega_A = 2\pi \times 1.0 \text{ THz}$ allows the resonance to be found in a search time T_A with signal-to-noise ratio [44]

$$\text{SNR} = (10.2 \pm 1.2) \left(\frac{S_{\text{IR}}}{2.83 \times 10^{-5} \text{ m}^2} \right) \left(\frac{B_{\text{DC}}}{1 \text{ T}} \right)^2 \left(\frac{D}{1 \text{ cm}} \right)^2 \left(\frac{L}{100 \text{ cm}} \right) \times \left(\frac{\Delta\nu_{\text{IR}}}{1 \text{ MHz}} \right)^{-1/2} \left(\frac{T_A}{17.4 \text{ hr}} \right)^{1/2} \left(\frac{\text{NEP}_A}{5.3 \times 10^{-13} \text{ W/Hz}^{1/2}} \right)^{-1}, \quad (9.2)$$

where, D is the laser beam diameter used to tune the cavity, L is the length of the bend magnet, and NEP_A is the noise equivalent power of the infrared detector at the Compton wavelength of dark matter $\lambda_A = (2.44 \pm 0.02) \mu\text{m}$. For typical detector [45] and magnet [46] parameters, the signal-to-noise ratio suffices to directly detect the resonant conversion of dark matter to infrared photons and measure the mass of the axions with precision $2\pi\Delta\nu_{\text{IR}}/\omega_A = 8.2 \text{ ppb}$ using a typical line-width $\Delta\nu_{\text{IR}} = 1 \text{ MHz}$ [39] and a search time $T_A = 17.4 \text{ hr}$ taking less than a day.

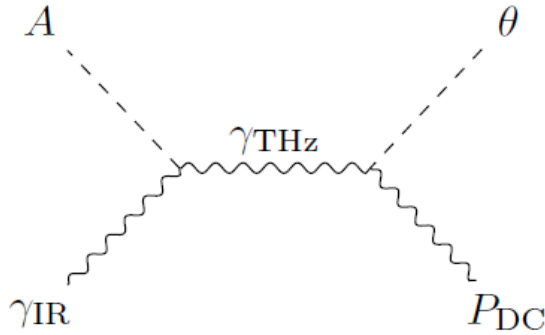


Figure 3. Halo axion A converts infrared photon γ_{IR} into terahertz photon γ_{THz} resonant with electromagnon θ in ferroelectric antiferromagnet with polarization P_{DC} .

10 Electromagnon Haloscopy

Figure 3 shows how the axion allows infrared light to excite electromagnons in ferroelectric antiferromagnets such as BiFeO_3 [47]. At room temperature the strongest electromagnon resonance in BiFeO_3 lies in the terahertz regime at frequency $\omega_\theta = 2\pi \times 0.54 \text{ THz}$ [48]. Looking in the infrared, we expect to see the electromagnon resonance as an absorption line in transmission through a sample provided the infrared light is detuned by ω_θ from the axion frequency $\omega_A = m_A = 2\pi \times (122.7 \pm 1.0) \text{ THz}$ [49].

Measuring the infrared frequency $\omega_{A\theta} = \omega_A - \omega_\theta$ that resonantly excites the electromagnon provides a table-top determination of the mass of the axion. For a thin sample, the dip in infrared transmission on resonance at $\omega_{A\theta}$ is set by the infrared refractive index $n(\omega_{A\theta})$ and the infrared absorption coefficient [50]:

$$\begin{aligned}
 \alpha(\omega_{A\theta}) &= \alpha(\omega_\theta) (n(\omega_{A\theta}))^2 m_A^4 g_{A\gamma\gamma}^2 |\tilde{\phi}_A(q_A)|^2 & (10.1) \\
 &= \alpha(\omega_\theta) (n(\omega_{A\theta}))^2 \left(\frac{\Delta a_\mu}{a_\mu} \right)^2 \frac{n_\theta V_\theta}{N_\mu} \frac{V_\theta}{V_\mu} \frac{T_\theta}{T_\mu} \\
 &= (12.4 \pm 1.5) \text{ cm}^{-1} \left(\frac{\alpha(\omega_\theta)}{10^7 \text{ cm}^{-1}} \right) \left(\frac{n(\omega_{A\theta})}{10} \right)^2 \\
 &\quad \times \left(\frac{n_\theta}{1.6 \times 10^{22} \text{ cm}^{-3}} \right) \left(\frac{V_\theta}{7.1 \times 10^{-3} \text{ cm}^3} \right)^2 \left(\frac{T_\theta}{30 \text{ ps}} \right),
 \end{aligned}$$

where, n_θ is the density of electrons participating in the electromagnon mode, V_θ is the volume of the infrared beam within an optically thin sample, and $T_\theta = 1/\Delta\omega_\theta$ is the coherent life-time of the electromagnon with line-width $\Delta\omega_\theta$ and terahertz absorption coefficient $\alpha(\omega_\theta)$. Using typical electromagnon parameters [51], we find the infrared absorption coefficient of the resonance that yields the mass of the dark matter is large enough to be seen in currently available samples of BiFeO_3 and related materials.

11 Conclusion

We conclude that the tensions between measurements of muon spin precession and standard model calculations are due to axions from the local dark matter halo of the galaxy. The resolution of the muon tension rests on a novel physical picture for the nature of dark matter. The picture leads to percent level predictions for the mass of the axion and for its coupling to electromagnetic fields provided that dark matter is made of axions.

Using kaon decays, we showed that dark matter in the local halo of the galaxy is made of axions. The observed charge asymmetry in kaon decays agrees with the asymmetry created by axions provided the axions have energy density that matches that of the local dark matter halo. The agreement suggests that the kaon decay asymmetry is due to axions in the local dark matter halo and that the local halo is made of axions.

The shift in the muon spin precession frequency due to axions from the local dark matter halo depends not just on the local axion energy density but also on the axion mass and electromagnetic coupling strength. For the mass of the axion predicted by our novel physical picture of the nature of dark matter, the predicted shift in the muon spin precession explains about half the observed tension between precession measurements and calculations based on measurements of the hadronic contribution. The other half of the tension follows from the analogous shift by axions of the measurements of the hadronic contribution: Axions from the local dark matter halo convert the neutral vector meson that dominates photon-hadron interactions into its slightly heavier and less dominant isoscalar cousin. Combining the two axion shifts, we resolve the muon tension and provide support for the conclusion that dark matter is made of axions with the predicted mass.

We have proposed table-top experiments to confirm that dark matter is made of axions. We predict a temperature shift of the proton spin precession frequency in liquids and a density shift of the electron transition frequency in optical lattice clocks. The predicted size of both effects is large enough to be seen with presently available table-top experiments.

To directly measure the mass of the axion, we propose to beat dark matter from the local halo against infrared light at the predicted Compton wavelength. The interference creates electromagnetic waves that excite the electromagnon mode in materials such as the room-temperature multiferroic material BiFeO_3 and that drive electron cyclotron motion in a magnetically confined laboratory plasma. The predicted size of the resonant infrared electromagnon absorption coefficient and the predicted size of the electron cyclotron resonance heating in the plasma are both large enough to be seen in currently available table-top experiments.

Finally, we have proposed to use a bend magnet to create infrared photons and to use a microwave cavity to absorb such photons from axions in the local dark matter halo of the galaxy. Measuring the frequency of the infrared photons created by the magnet and absorbed by the cavity gives the mass of dark matter with more than twice the precision of the mass of the muon in searches that take less than a day with the magnet and less than a month with the cavity. These table-top experiments would confirm the proposed form of dark matter with the predicted mass.

Acknowledgements

This research was supported in part by the National Science Foundation under Grant No. NSF PHY-1748958, by the Department of Energy under grant No. DE-FG02-00ER41132, and by the Mainz Institute of Theoretical Physics within the Cluster of Excellence PRISMA+ (Project ID 39083149).

Open Access. This article is distributed under the terms of the Creative Commons Attribution License ([CC-BY 4.0](#)), which permits any use, distribution and reproduction in any medium, provided the original author(s) and source are credited. SCOAP³ supports the goals of the International Year of Basic Sciences for Sustainable Development.

References

- [1] J. Schwinger, *On Quantum-Electrodynamics and the Magnetic Moment of the Electron*, Phys. Rev. **73** (1948) 416.
- [2] B. Abi, T. Albahri, S. Al-Kilani, D. Allspach, L. P. Alonzi et al. (Muon $g - 2$ Collaboration), *Measurement of the Positive Muon Anomalous Magnetic Moment to 0.46 ppm*, Phys. Rev. Lett. **126** (2021) 141801.
- [3] G.W. Bennett, B. Bousquet, H. N. Brown, G. Bunce, R. M. Carey et al. (Muon $g - 2$ Collaboration), *Final report of the muon E821 anomalous magnetic moment measurement at BNL*, Phys. Rev. D **73** (2006) 072003.
- [4] F. Jegerlehner, *The Anomalous Magnetic Moment of the Muon*, 2nd ed., Springer-Verlag, Berlin (2017).
- [5] T. Aoyama, N. Asmussen, M. Benayoun, J. Bijnens, T. Blum et al., *The anomalous magnetic moment of the muon in the standard model*, Phys. Rep. **887** (2020) 1.
- [6] Sz. Borsanyi, Z. Fodor, J. N. Guenther, C. Hoelbling, S. D. Katz et al., *Leading hadronic contribution to the muon magnetic moment from lattice QCD*, Nature **593** (2021) 51.
- [7] P. A. Zyla et al. (Particle Data Group), *Review of Particle Physics*, Prog. Theor. Exp. Phys., **2020** (2020) 083C01.
- [8] S. Bennett et al., Phys. Rev. Lett. **19** (1967) 993.
- [9] J. Marx et al., Phys. Lett. B **32** (1970) 219.
- [10] V. L. Fitch et al. Phys. Rev. Lett. **31** (1973) 1524.
- [11] C. Geweniger et al., Phys. Lett. B **48** (1974) 483.
- [12] A. Alavi-Harati et al. (FNAL KTeV Collab.), Phys. Rev. Lett. **88** (2002) 181601.
- [13] The axions A_M are constructed to transform under C , P , and T as follows:

$$CA_M = A_M, \quad PA_M = -A_M, \quad TA_M = -A_M.$$

To check that they do so, recall that quarks and leptons M_H^P transforms as follows:

$$CM_H^P = \overline{M}_H^{\overline{P}}, \quad PM_H^P = M_{\overline{H}}^P, \quad TM_H^P = \overline{M}_{\overline{H}}^{\overline{P}}.$$

[14] For anti-matter, the meaning of the parity check is reversed compared to matter: $P = +$ indicates anti-quarks and anti-leptons which *do* feel the weak force, while $P = -$ means the anti-matter *does not* feel it. Nevertheless, the standard model correlation between helicity $H = L, R$ and parity check $P = +, -$ applies in the same way to anti-matter as it does to matter: \overline{M}_L^- and \overline{M}_R^+ occur in the standard model while neither \overline{M}_L^+ nor \overline{M}_R^- do. See, for example, the discussion in Ref. [52] on pgs. 704–705.

[15] There are $|M| = 12$ flavors of matter in the standard model of particle physics. They fall into three “generations” each containing a pair of quarks and a pair of leptons. See the discussion in Ref. [52] on pgs. 703–705, 707, and 721 for a detailed description of the matter content of the Standard Model in the language of quantum field theory. The ratio of the energy density parameters $\Omega_A h^2 / (\Omega_\gamma h^2) = u_A / u_\gamma$ gives the ratio of the energy per volume $u_A = m_A n_A$ stored in dark matter to the energy per volume $u_\gamma = 2.70 \times n_\gamma k T_\gamma$ stored in light energy. For a derivation, see P. J. E. Peebles, *Principles of Physical Cosmology*, Princeton University Press, Princeton, NJ (1993), pgs. 137–138, 158–160. The Boltzmann constant is [53]:

$$k = 1.380\,649 \times 10^{-23} \text{ J/K (exact)} = 0.861\,733 \times 10^{-4} \text{ eV/K.}$$

[16] D. J. Fixsen, *The Temperature of the Cosmic Microwave Background*, *Astrophys. J.* **707** (2009) 916.

[17] N. Aghanim, Y. Akrami, M. Ashdown, J. Aumont, C. Baccigalupi et al. (Planck Collaboration), *Planck 2018 Results VI. Cosmological Parameters*, *A&A* **641** (2018) A6. We use parameters from the baseline model fit to the most complete combination of available data. The results are given in *Planck 2018 Results: Cosmological Parameter Tables*, pg. 49 (May 14, 2019).

[18] The rate $\Gamma(\pi^- e^+ \nu_e)$ of the decay of the long-lived neutral kaon K_L^0 to a negative pion π^- , a positron e^+ , and an electron neutrino ν_e is larger than the rate $\Gamma(\pi^+ e^- \bar{\nu}_e)$ for the charge conjugate reaction due to the charge asymmetry [7]:

$$A_L(e) = (\Gamma(\pi^- e^+ \nu_e) - \Gamma(\pi^+ e^- \bar{\nu}_e)) / (\Gamma(\pi^- e^+ \nu_e) + \Gamma(\pi^+ e^- \bar{\nu}_e)) = (3.34 \pm 0.07) \times 10^{-3}.$$

The axion field strength $|\tilde{\phi}_A(q_A)|^2 \approx \phi_A^2 V_K T_K$ is fixed by the axion energy density $\rho_A = \phi_A^2 m_A^2$ where ϕ_A is the axion amplitude as a function of position [20]. The kaon volume $V_K = \pi L_K (h/p_K)^2$ and the kaon time $T_K = L_K/c$ give the size of the region of space-time within the decay volume where the axion and kaon interact coherently. The following exact values for the defining constants of the international system (SI) appear in the expression for $A_L(e)$ and/or in its numerical evaluation [53]:

$$\begin{aligned} c &= 299\,792\,458 \text{ m/s,} \\ h &= \hbar \times 2\pi = 6.626\,070\,15 \times 10^{-34} \text{ J s,} \\ e &= 1.602\,176\,634 \times 10^{-19} \text{ C.} \end{aligned}$$

[19] J. L. Rosner, S. L. Stone and R. Van de Water, *71. Leptonic decays of charged pseudoscalar mesons*, pg. 803 in Ref. [7] gives the result $|V_{ud}| f_\pi \times \sqrt{2} = 127.13 \pm 0.13$ MeV where $|V_{ud}| = 0.973\,70 \pm 0.000\,14$ is the light quark mixing amplitude [54]. Combining we find $f_\pi = (92.32 \pm 0.09)$ MeV for the pion decay constant.

[20] R. D. Peccei, in *CP Violation*, ed. C. Jarlskog, World Scientific, Singapore (1989), pgs. 525–532.

[21] $C_{A\pi}$ follows from the way the axion shifts $U_\theta \phi_A = \phi_A + 2\theta f_A$ under the axial twist $U_\theta M_H^P = e^{-iP\theta} M_H^P$ in the phase of matter that feels the weak nuclear force M_H^- relative to

the phase of matter M_H^+ that does not feel this force. See Ref. [20] for $C_{A\pi}$ in terms of the light quark masses and the way the axion shifts under the axial twist. See Ref. [55] for the light quark mass ratio $m_u/m_d = 0.485 \pm 0.019$.

- [22] M. Gorgetto and M. Villadoro, *Topological susceptibility and QCD axion mass: QED and NNLO corrections*, J. High Energ. Phys. **2019** (2019) 33.
- [23] A.-C. Eilers, D. W. Hogg, H.-W. Rix, and M. K. Ness, *The Circular Velocity Curve of the Milky Way from 5 to 25 kpc*, Astrophys. J. **871** (2019) 120.
- [24] Using the value for $\rho_A = (0.28 \pm 0.03)$ GeV/cm³ determined by the best available $A_L(e)$ measurement in Ref. [12], one can use Eq. (3.1) to predict the charge asymmetry observed in other experiments given the length L_K of their decay volume. For example, the first such measurement $A_L(e) = (2.24 \pm 0.36) \times 10^{-3}$ [8] had length $L_K = 375$ cm which yields $A_L(e) = (2.46 \pm 0.17) \times 10^{-3}$ using Eq. (3.1) in pleasing agreement with the observed charge asymmetry despite the well-known tension of this first measurement with the current world average. The difference in the length L_K resolves the tension. The rough similarity in the length $L_K \approx 500$ cm of the measurements that enter the current world average for which published scale drawings of the decay volume are available [9, 11, 12] explains the consistency of their results for $A_L(e)$ given the relation with L_K expressed in Eq. (3.1).
- [25] The axion ϕ_A couples to photons via the term in the action

$$\mathcal{S}_{A\gamma} = \int d^3x dt g_{A\gamma\gamma} \phi_A \mathbf{E} \cdot \mathbf{B}$$

where, \mathbf{E} is the electric field and \mathbf{B} is the magnetic field. We follow here the conventions of Ref. [20] in which the “free” terms in the axion action take the form

$$\mathcal{S}_A = \int d^3x dt \left[(1/2)(\partial_t \phi_A)^2 - (1/2)(\nabla \phi_A)^2 - (1/2)m_A^2 \phi_A^2 \right].$$

- [26] Under C , PT and CPT , the shift Δa_μ , like the axion amplitude, does not change sign.
- [27] The axion-photon coupling is given by the following expression [20, 25]:

$$g_{A\gamma\gamma} = C_{A\gamma} \frac{\alpha}{2\pi} \frac{1}{f_A} = (0.68 \pm 0.02) \times 10^{-10} \text{ GeV}^{-1}. \quad (11.1)$$

Here, the fine-structure constant enters [53]:

$$\alpha = (7.297\ 352\ 5693 \pm 0.000\ 000\ 00011) \times 10^{-3}. \quad (11.2)$$

The mass of the axion m_A and the product $m_A f_A = \sqrt{\chi_{\text{QCD}}}$ which is fixed by the topological susceptibility χ_{QCD} of the quantum chromodynamic vacuum combine to give the axion decay constant [22]:

$$f_A = \frac{m_A f_A}{m_A} = \frac{(5.69 \pm 0.05) \times 10^{-3} \text{ GeV}^2}{(0.508 \pm 0.004) \text{ eV}} = (1.120 \pm 0.010) \times 10^7 \text{ GeV}. \quad (11.3)$$

Finally, the light quark mass ratio $m_u/m_d = 0.485 \pm 0.019$ [55] gives the dimensionless constant [20, 25]:

$$C_{A\gamma} = \frac{8}{3} - \frac{2}{3} \frac{4m_d + m_u}{m_d + m_u} = 0.653 \pm 0.017. \quad (11.4)$$

- [28] For the muon beam at Fermilab E989 (FNAL) [2], the volume is

$$V_\mu = 2\pi^2 R \sigma_x \sigma_y = 3.12 \times 10^4 \text{ cm}^3,$$

where, $R = 711$ cm is the radius of the central orbit of muons in the ring, $\sigma_x = 1.78$ cm is the radial width of the beam, and $\sigma_y = 1.25$ cm is the vertical width [2, 56, 57]. The average number of muons is

$$N_\mu = \frac{4}{9} N_0 e^{-t_{\text{fill}}/(\gamma \tau_\mu)} \approx \frac{4}{9} \times 4340 = 1930,$$

where, $N_0 \approx 6920$ is the number of muons in the ring at the start of the fill, and $t_{\text{fill}} \approx 30$ μsec is the time it takes to fill the ring [2, 56]. The muon life-time in the haloscope rest frame is $T_\mu = \gamma_\mu \tau_\mu = 64.4$ μsec , where, $\gamma_\mu \approx p_\mu/(m_\mu c) = 29.3$ is the muon time dilation factor, $p_\mu = 3.10$ GeV/c is the muon momentum, $m_\mu = 0.106$ GeV/c² is the muon rest mass, and $\tau_\mu = 2.20$ μsec is the muon life-time at rest [2]. For the measurements at Brookhaven E821 (BNL) [3], we estimate $N_\mu = 1290$, $\sigma_x = 2.10$ cm, $\sigma_y = 1.53$ cm (J. Mott, private communication). To find the shift of muon spin precession from halo axions, we first computed $|\Delta a_\mu(\text{FNAL})| = (165 \pm 10) \times 10^{-11}$ and $|\Delta a_\mu(\text{BNL})| = (161 \pm 10) \times 10^{-11}$ for each experiment using Eq. (3). Next we took the average of the two experiments to obtain Δa_μ , since the shifts essentially agree.

- [29] We follow the analysis reviewed in Ref. [20] and set the ratio of axion couplings $g_{A\rho\omega}/g_{A\gamma\gamma} = g_{\rho\omega}/g_{\gamma\gamma}$ to match that of the neutral pion. Vector meson dominance [58] gives the pion ratio in terms of the ρ and ω vector meson partial widths for electron-positron pair production, as shown in Eq. (4). The electron-positron quantities entering Eq. (4) may be expressed in terms of the collider parameters: $V_\rho = 8\pi\sigma_x\sigma_y\sigma_z$ where $\sigma_x, \sigma_y, \sigma_z$ are the horizontal, vertical, and longitudinal sizes of the bunch at the interaction point, $T_\rho = 2\sigma_z/c$, and the ρ^0 vector meson has momentum $p_\rho = (E^2 - m_\rho^2)/(2E)$ in the lab frame for annihilation of electrons and positrons with equal beam energies $E_+ = E_- = E/2$ that collide after emitting a photon with energy $E - m_\rho$. For example, the DAΦNE collider had $E_+ = E_- = m_\phi/2 = 510$ MeV and used initial state radiation to reach the ρ^0 vector meson resonance for $\pi^+\pi^-$ creation from e^+e^- annihilation [59]. For energy scan experiments, the collision energy $E \approx m_\rho$ lands on the ρ^0 vector meson resonance, and, as a result, the ρ^0 vector meson has lab-frame momentum $p_\rho = \sqrt{2} \times \Delta E$ set by the spread ΔE in the beam energy.
- [30] The meson parameters are as follows [7]:

$$\begin{aligned} m_\rho &= 775 \text{ MeV}, \\ m_\omega &= 783 \text{ MeV}, \\ \Gamma_\rho^{ee} &= \Gamma_\rho \times \text{B.R.}(\rho \rightarrow e^+e^-) = (147 \text{ MeV})(4.72 \times 10^{-5}) = 6.94 \text{ keV}, \\ \Gamma_\omega^{ee} &= \Gamma_\omega \times \text{B.R.}(\omega \rightarrow e^+e^-) = (8.68 \text{ MeV})(7.38 \times 10^{-5}) = 0.641 \text{ keV}. \end{aligned}$$

Using the meson parameters, we can find the vector meson coupling strengths [58]:

$$\begin{aligned} g_\rho^2/(4\pi) &= \alpha^2 m_\rho / (3\Gamma_\rho^{ee}) = 1.98, \\ g_\omega^2/(4\pi) &= \alpha^2 m_\omega / (3\Gamma_\omega^{ee}) = 21.7. \end{aligned}$$

These coupling strengths then give the ratio of the axion-meson coupling to the axion-photon coupling [20, 58]:

$$\frac{g_{A\rho\omega}}{g_{A\gamma\gamma}} = \frac{1}{\alpha} \sqrt{\frac{g_\rho^2}{4\pi} \frac{g_\omega^2}{4\pi}} = 8.98 \times 10^2.$$

The axion coupling ratio allows us to evaluate the drop in the hadronic contribution (See Eq.

4):

$$\begin{aligned}\Delta a_\mu^{\text{HLO}} &= \Delta a_\mu \left(\frac{a_\mu^{\text{HLO}}}{a_\mu} \right) \left(\frac{p_\rho}{m_A} \right) \left(\frac{g_{A\rho\omega}}{g_{A\gamma\gamma}} \right) \sqrt{\frac{1}{N_\mu} \frac{V_\rho}{V_\mu} \frac{T_\rho}{T_\mu}} \\ &= 0.170 \times \Delta a_\mu (\text{FNAL}) \left(\frac{p_\rho}{100 \text{ MeV}} \right) \left(\frac{V_\rho}{10^{-2} \text{ cm}^3} \right)^{1/2} \left(\frac{T_\rho}{100 \text{ psec}} \right)^{1/2},\end{aligned}$$

where, we have approximated the standard model value for the muon spin precession by the leading order electromagnetic contribution $a_\mu \approx \alpha/(2\pi) \approx 1.16 \times 10^3$ [1, 4, 5]. Similarly, we approximate the standard model value for the hadronic contribution to muon spin precession $a_\mu^{\text{HLO}} = 700 \times 10^{-10}$ [5, 6]. The muon beam parameters N_μ , V_μ , and T_μ are those of the FNAL E989 spin precession experiment [28]. Hadron production by the DAΦNE collider detected by KLOE at the ρ^0 vector meson $\pi^+\pi^-$ resonance lies close to the world average for this channel which dominates the a_μ^{HLO} calculation within the standard model [5]. We therefore estimate the shift $\Delta a_\mu^{\text{HLO}}$ using the electron-positron beam parameters inside KLOE at DAΦNE [59]:

$$\sigma_x = 0.2 \text{ cm}, \sigma_y = 2 \times 10^{-3} \text{ cm}, \sigma_z = 3 \text{ cm}, E_+ = E_- = 510 \text{ MeV}.$$

Combining the electron-positron beam parameters using the expressions in [29], one finds $V_\rho = 3.0 \times 10^{-2} \text{ cm}^3$, $T_\rho = 200 \text{ psec}$, and $p_\rho = 219 \text{ MeV}$. Finally, we get the shift of the hadronic contribution at KLOE:

$$\Delta a_\mu^{\text{HLO}} (\text{KLOE}) = 0.170 \times (165 \pm 10) \times 10^{-11} \times 2.19 \times \sqrt{(3.0)(2.0)} = (148 \pm 9) \times 10^{-11},$$

where, we have used the shift $\Delta a_\mu (\text{FNAL})$ predicted using FNAL E989 beam parameters [28].

[31] Figure 1 shows the leading order quantum electrodynamic radiative correction to the electromagnetic vertex of the proton in water [60]:

$$\Delta g'_{p,\text{EM}} = \frac{\alpha}{\pi\epsilon} \approx \frac{1}{137 \times \pi \times 78.4} \approx 2.96 \times 10^{-5}. \quad (11.5)$$

This correction dominates the axion shift since the axion needs to couple to a virtual photon. By contrast, hadronic contributions dominate the full radiative correction to the electromagnetic vertex of the proton in liquid water [32]:

$$(g'_p - 2)/2 \approx 2.79 - 1 = 1.79. \quad (11.6)$$

Despite dominating the full electromagnetic vertex correction, these hadronic contributions do not contain the necessary virtual photon. Thus, they make a sub-dominant contribution to the axion shift of the proton spin precession frequency in water.

[32] W. D. Phillips, W. E. Cooke and D. Kleppner, *Magnetic Moment of the Proton in H₂O in Bohr Magnetons*, Phys. Rev. Lett. **35** (1975) 1619; *ibid.* **36** (1976) 689 and 1473.
[33] The bulb of liquid water in Ref. [32] was a sphere of diameter 1.3 cm with volume

$$V_p = (4\pi/3)(1.3/2)^3 \text{ cm}^3 = 1.15 \text{ cm}^3. \quad (11.7)$$

The proton resonance line-width $\Delta\omega'_p = 2\pi \times 1.5 \text{ Hz}$ due to variation in the field strength over the sample volume gave effective spin coherence time

$$T_p \approx 1/\Delta\omega'_p = 0.11 \text{ sec.} \quad (11.8)$$

The temperature of the bulb $T = (34.7 \pm 0.1)^\circ\text{C} = 308 \text{ K}$ gave proton spin polarization

$$P_p = \frac{\hbar\omega'_p}{kT} = \frac{4.14 \times 10^{-9} \text{ eV/MHz} \times 15 \text{ MHz}}{0.862 \times 10^{-4} \text{ eV/K} \times 308 \text{ K}} = 2.34 \times 10^{-6}, \quad (11.9)$$

where, the precession frequency was $\omega'_p = 2\pi \times 42.8 \text{ MHz}/T \times 0.35 \text{ T} = 15 \text{ MHz}$ in magnetic field $B = 0.35 \text{ T}$ [32]. Using the proton volume V_p and proton polarization P_p , we find the effective proton number

$$\begin{aligned} N_p &= n_p V_p P_p \\ &= (6.69 \times 10^{22} \text{ cm}^{-3}) \times (1.15 \text{ cm}^3) \times (2.34 \times 10^{-6}) \\ &= 1.80 \times 10^{17}, \end{aligned} \quad (11.10)$$

where, we have used the proton number density in liquid water

$$n_p = (1.00 \text{ g/cm}^3)(6.02 \times 10^{23} \text{ H}_2\text{O}/18.0 \text{ g})(2 \text{ p/H}_2\text{O}) = 6.69 \times 10^{22} \text{ cm}^{-3}. \quad (11.11)$$

Using Eq. (5.1), we find the shift of the proton spin precession frequency in water:

$$\begin{aligned} \Delta g'_p &= 2 \times \frac{(165 \pm 10) \times 10^{-11}}{78.4} \left(\frac{1.80 \times 10^{17}}{1.93 \times 10^3} \right)^{1/2} \left(\frac{1.15 \text{ cm}^3}{3.12 \times 10^4 \text{ cm}^3} \right)^{1/2} \left(\frac{0.11 \text{ sec}}{64.4 \times 10^{-6} \text{ sec}} \right)^{1/2} \\ &= (1.02 \pm 0.06) \times 10^{-4} \left(\frac{V_p}{1.15 \text{ cm}^3} \right) \left(\frac{T_p}{308 \text{ K}} \right)^{-1/2} \left(\frac{\Delta\omega'_p}{10^{-7} \omega'_p} \right)^{-1/2}, \end{aligned} \quad (11.12)$$

where, $\epsilon = 78.4$ [60] is the static dielectric constant in water and we have taken the muon beam parameters N_μ, V_μ, T_μ and the predicted shift Δa_μ from the Fermilab E989 muon spin precession measurement [28]. Taking the temperature derivative, we find the slope

$$\frac{1}{g'_p} \frac{dg'_p}{dT} = -\frac{1}{2} \frac{\Delta g'_p}{g'_p T} = -(29.7 \pm 1.8) \frac{\text{ppb}}{\text{K}} \left(\frac{V}{1.15 \text{ cm}^3} \right) \left(\frac{T}{308 \text{ K}} \right)^{-3/2} \left(\frac{\Delta\omega'_p}{10^{-7} \omega'_p} \right)^{-1/2}, \quad (11.13)$$

where, $g'_p \approx 5.58$ gives the slope in parts per billion (ppb) of g'_p [32].

- [34] The internal magnetic field felt by valence electrons in their rest-frame is created within high atomic number atoms by the motion of the electrons at close to the speed of light through the static internal electric field created by the nucleus of the atom and screened by the core electrons.
- [35] Atoms with mass m and temperature T moving in the optical lattice trap of radius r and height z trace out the volume

$$\begin{aligned} V_a &= \pi r^2 z = \sqrt{2} \pi^2 \left(\frac{w}{\lambda_L} \right)^2 \left(\frac{\lambda_L}{2\pi} \right)^3 \left(\frac{kT}{V_0} \right)^{3/2} \\ &= 5.5 \times 10^{-12} \text{ cm}^3 \left(\frac{T}{9 \mu\text{K}} \right)^{3/2} \left(\frac{V_0}{200 E_R} \right)^{-3/2} \left(\frac{E_R}{h \times 2.0 \text{ kHz}} \right)^{-3} \left(\frac{m}{171 m_p} \right)^{-3/2} \left(\frac{w}{26.4 \lambda_L} \right)^2, \end{aligned} \quad (11.14)$$

where, the lattice photons have wavelength λ_L , the lattice laser has beam waist w , and the lattice has depth V_0 expressed in terms of the lattice recoil energy $E_R = \hbar^2/(2m\lambda_L^2)$. The thermal motion of the ultracold atoms in the trap has coherence time $T_a = \hbar/(kT)$ set by the temperature of the atoms.

- [36] T. Kobayashi, A. Takamizawa, D. Akamatsu, A. Kawasaki, A. Nishiyama, K. Hosaka, Y. Hisai, M. Wada, H. Inaba, T. Tanabe, and M. Yasuda, *Search for ultralight dark matter from*

long-term frequency comparisons of optical and microwave atomic clocks, Phys. Rev. Lett. **129** (2022) 241301. For the observations of the density shift of the optical lattice clock frequency with roughly the size predicted by Eq. (6.2), see Section 1.2 of the Supplementary Materials. The lattice photon wavelength $\lambda_L = 759$ nm gives recoil energy $E_R = h \times 2.0$ kHz for ytterbium-171 atoms which have mass $m = 171 m_p$. The lattice had depth $V_0 = 200 E_R = 0.47 kT$ for atoms which typically had temperature $T = 9 \mu\text{K}$. The lattice laser beam had waist $w = 26.4 \lambda_L = 20 \mu\text{m}$ and there were typically $N_a = 100$ atoms in the trap (T. Kobayashi, private communication). In the main paper, the authors use $k_\alpha = -2.59$ for the sensitivity to changes in the fine-structure constant for the line ratio $\nu_{\text{Yb}}/\nu_{\text{Cs}}$ of the ytterbium optical lattice clock frequency to the cesium-133 microwave clock frequency. However, the density shift due to modulating the ytterbium atom number occurs at fixed ν_{Cs} . In that case, the appropriate sensitivity $k_\alpha \approx 0.24$ is simply that of the ytterbium transition frequency [61].

[37] In the presence of axions with amplitude $\tilde{\phi}_A(q_A)$, the equations of motion for the infrared magnetic field B_{IR} and the radio-frequency electric field E_{RF} have the following solution

$$E_{\text{RF}} = m_A^2 g_{A\gamma\gamma} \tilde{\phi}_A(q_A) B_{\text{IR}}, \quad (11.15)$$

where, the mass of the axion $m_A c^2/\hbar = \omega_A = \omega_{\text{IR}} + \omega_{\text{RF}}$ relates the frequency ω_{IR} of the infrared light and the frequency ω_{RF} of the radio waves. The radio-frequency power $P_{\text{RF}} = (1/2) \times E_{\text{RF}}^2/(2Z_0)$ with the polarization that excites the resonance is half of the total amount created by the unpolarized infrared power $P_{\text{IR}} = (B_{\text{IR}} c)^2/(2Z_0)$, where, $Z_0 = \sqrt{\mu_0/\epsilon_0} \approx 377 \Omega$ is the impedance of the vacuum.

[38] For light and electrons propagating along the magnetic field, only right-handed circularly polarized light is absorbed by the electron cyclotron motion. Left-handed light passes through without being absorbed. For an unpolarized incoming beam, the out-going beam has circular polarization $(P_L - P_R)/(P_L + P_R) = \Delta P_{\text{IR}}/P_{\text{IR}}$ given by Eq. 7.2, where, P_L is the left-handed and P_R is the right-handed transmitted infrared power. Electrons in a warm, magnetically confined plasma at temperature T and magnetic field strength B have density

$$n_e = \beta \frac{B^2}{2\mu_0 kT} = 2.0 \times 10^{17} \text{ cm}^3 \left(\frac{\beta}{0.8} \right) \left(\frac{T}{12,000 \text{ K}} \right)^{-1} \left(\frac{B}{0.32 \text{ T}} \right)^2, \quad (11.16)$$

where, $\mu_0 = 4\pi \times 10^{-7} \text{ T}^2 \text{ m}^3 \text{ J}^{-1}$ is the magnetic permeability of the vacuum [53], $k = 1.38 \times 10^{-23} \text{ J/K}$ [53] is the Boltzmann constant, and β is the ratio of the electron pressure to the magnetic energy density. Passing the plasma through the bore of a solenoid magnet gives the coherent volume

$$V_e = \pi (c/\omega_c)^2 L = 89 \text{ cm}^3 \left(\frac{B}{0.32 \text{ T}} \right)^{-2} \left(\frac{L}{100 \text{ cm}} \right), \quad (11.17)$$

where, ω_c is the cyclotron frequency, L is the length of the bore, and the laser beam waist is set by the reduced wavelength $c/\omega_c = 5.3 \text{ mm} (B/0.32 \text{ T})^{-1}$ of the radio-frequency electromagnetic waves at electron cyclotron resonance. The coherent line-width $\Delta\nu_{\text{IR}}$ of the infrared laser sets the coherence time

$$T_e = \frac{1}{2\pi\Delta\nu_{\text{IR}}} = 0.16 \text{ } \mu\text{sec} \left(\frac{\Delta\nu_{\text{IR}}}{1 \text{ MHz}} \right)^{-1}. \quad (11.18)$$

[39] The tunable continuous-wave external cavity diode laser (Sacher Lasertechnik TEC-500-2400-003-M) has infrared wavelength range 2300 nm – 2500 nm that includes the

predicted Compton wavelength of dark matter $\lambda_A = 2440 \pm 19$ nm and it has line-width $\Delta\nu_{\text{IR}} = 1$ MHz. For a recent demonstration of phase coherence with infrared laser beams enlarged to a radius ≈ 5 mm comparable to the beam waist $c/\omega_c = 5.3$ mm $(B/0.32 \text{ T})^{-1}$ needed to see dark matter with plasma haloscopy [38] and the beam diameter $D = 1$ cm needed for microwave [41] and bend magnet haloscopy [44], see Ref. [62], Supplementary Materials, pg. 2.

- [40] K. Hoshino, J. Nucl. Sci. and Tech. **27** (1990) 391 describes electron cyclotron heating in magnetically confined laboratory plasma with $\beta = 0.8$, $L = 100$ cm, $T = 12,000$ K, and $B = 0.32$ T.
- [41] The volume of the infrared beam $V_{\text{IR}} = (\pi/4)D^2L$ is fixed by the beam diameter D and the cavity length L . The coherence time $T_{\text{IR}} = 1/(2\pi\Delta\nu_{\text{IR}})$ comes from the infrared laser line-width $\Delta\nu_{\text{IR}}$. The radio-frequency power P_{IR} combines with the receiver noise temperature T_S and the integration time T_{int} to give the signal-to-noise ratio [63]

$$\text{SNR} = \frac{P_{\text{RF}}}{kT_S} \sqrt{\frac{T_{\text{int}}}{\Delta\nu_{\text{IR}}}}. \quad (11.19)$$

The total search time $T_A = T_{\text{int}}\Delta m_A c^2/(h\Delta\nu_{\text{IR}})$ is set by the width of the window $\Delta m_A c^2 = 4 \times 10^{-3}$ eV = $h \times 1.0$ THz for the axion mass given in Eq. 2.2.

- [42] The typical microwave cavity has length $L = 112$ cm and is read out by a receiver with noise temperature $T_S = 77$ K set by the boiling point of liquid nitrogen. See for example the cavity and receiver described in Ref. [64].
- [43] In the presence of axions with amplitude $\tilde{\phi}_A(q_A)$, the equations of motion for the infrared electric field E_{IR} and the static magnetic field B_{DC} have the following solution

$$E_{\text{IR}} = m_A^2 g_{A\gamma\gamma} \tilde{\phi}_A(q_A) B_{\text{DC}}, \quad (11.20)$$

where, the mass of the axion $m_A c^2/\hbar = \omega_A = \omega_{\text{IR}}$ gives the frequency of the infrared light and the impedance $Z_0 = \sqrt{\mu_0/\epsilon_0} \approx 377 \Omega$ [53] of the vacuum gives the infrared power $P_{\text{IR}} = E_{\text{IR}}^2/(2Z_0)$. The infrared electric field E_{IR} is polarized along the static magnetic field B_{DC} .

- [44] The infrared cavity fills the volume $V_B = (\pi/4)D^2L$ within the bend magnet of length L defined by the beam diameter D of the infrared laser used to tune the cavity. The tune laser is polarized with its electric field perpendicular to the static magnetic field B_{DC} and a crossed linear polarizer oriented parallel to B_{DC} at the cavity exit transmits to the photodiode reading out the infrared power P_{IR} only the infrared photons created within the cavity by dark matter. The infrared cavity has coherence time $T_{\text{IR}} = 1/(2\pi\Delta\nu_{\text{IR}})$ when it is tuned to a laser with line-width $\Delta\nu_{\text{IR}}$. For each frequency in the window $\Delta\omega_A = 2\pi \times 1.0$ THz around the dark matter resonance $\omega_A = 2\pi \times (122.7 \pm 1.0)$ THz, we have integration time $T_{\text{int}} = T_A \times \Delta\omega_A/(2\pi\Delta\nu_{\text{IR}})$, where T_A is the total time taken to scan the window assuming T_{int} is much longer than the time it takes to lock the cavity to the laser at a given wavelength.
- [45] The two-stage thermoelectrically cooled indium gallium arsenide photodiode (Hamamatsu G12183-230K) with photosensitive area $S_{\text{IR}} = \pi \times (3 \text{ mm})^2 = 2.83 \times 10^{-5} \text{ m}^2$ has typical noise equivalent power $\text{NEP}_A = (1.15/1.3) \times \text{NEP}_{\text{peak}} = 5.3 \times 10^{-13} \text{ W/Hz}^{1/2}$ at the Compton wavelength of dark matter $\lambda_A = (2.44 \pm 0.02) \mu\text{m}$, where NEP_{peak} is the typical value for the most photosensitive wavelength $\lambda_{\text{peak}} \approx 2.3 \mu\text{m}$ in the photodiode's spectral

response range from $0.9 \mu\text{m}$ to $2.55 \mu\text{m}$. For integration time T_{int} , we get the signal-to-noise ratio $\text{SNR} = P_{\text{IR}} T_{\text{int}}^{1/2} / \text{NEP}_A$.

- [46] Typical magnetic dipole bend magnets have magnetic field strength $B_{\text{DC}} = 1 \text{ T}$ and length $L = 100 \text{ cm}$. See for example Ref. [65] in which an infrared optical cavity was created within a bend magnet from the proton storage ring of the former HERA electron-proton collider at DESY in Hamburg.
- [47] R. de Sousa and J. E. Moore, *Optical coupling to spin waves in the cycloidal multiferroic BiFeO₃*, Phys. Rev. B **77** (2008) 012406.
- [48] D. Talbayev, S. A. Trugman, Seongsu Lee, Hee Taek Yi, S.-W. Cheong, and A. J. Taylor, *Long-wavelength magnetic and magnetoelectric excitations in the ferroelectric antiferromagnet BiFeO₃*, Phys. Rev. B **83** (2011) 094403.
- [49] The electromagnon θ resonates when the terahertz electric field E_{THz} is perpendicular to the spin cycloid plane in BiFeO₃. This plane is defined by the spontaneous polarization P_{DC} and the cycloid wavevector: See Eq. (10), Fig. 2, and accompanying discussion on pg. 3 of Ref. [47]. The axion converts the magnetic field B_{IR} in the incident infrared light into a parallel terahertz frequency electric field E_{THz} . The infrared light gets absorbed when E_{THz} resonates with the electromagnon θ . This happens when B_{IR} is perpendicular to the spin cycloid plane.
- [50] The absorption coefficient $\alpha(\omega)$ for electromagnetic waves of frequency ω gives the attenuation rate for the decrease of the transmitted light intensity $I(z) = I_0 \exp(-\alpha(\omega)z)$ as a function of the thickness z of the sample for incident light with intensity I_0 . See M. Dressel and G. Gruner, *Electrodynamics of Solids*, Cambridge University Press, Cambridge, UK (2002), pg. 26. Similarly, the refractive index $n(\omega)$ gives the wavevector $k(\omega) = n(\omega)\omega/c$ for electromagnetic waves of frequency ω , where, c is the vacuum speed of light. See *ibid.*, pg. 24.
- [51] The typical room-temperature electromagnon absorption coefficient is $\alpha(\omega_\theta) = 10^7 \text{ cm}^{-1}$ while the index of refraction is $n(\omega_{A\theta}) = 10$ [48]. The electrons that participate in the electromagnon in BiFeO₃ have density

$$n_\theta = \frac{\rho N_A}{\mu} = \frac{(8.22 \text{ g/cm}^3)(6.02 \times 10^{23})}{313} = 1.58 \times 10^{22} \text{ cm}^3, \quad (11.21)$$

where, ρ is the mass density of BiFeO₃, N_A is the Avogadro number [53], and μ is the molar mass of BiFeO₃. The typical electromagnon line-width $\Delta\nu_\theta \approx 5.3 \text{ GHz}$ [48] at room temperature sets the coherent life-time

$$T_\theta = \frac{1}{2\pi\Delta\nu_\theta} = 30 \text{ ps} \left(\frac{\Delta\nu_\theta}{5.3 \text{ GHz}} \right)^{-1}. \quad (11.22)$$

The diameter $d = 0.3 \text{ cm}$ of a ferroelectric domain within a single crystal sample sets the spot size for the light shining through the sample of thickness $t = 0.1 \text{ cm}$ to give the coherent volume

$$V_e = \frac{1}{4}\pi d^2 t = 7.1 \times 10^{-3} \text{ cm}^3 \left(\frac{d}{0.3 \text{ cm}} \right)^2 \left(\frac{t}{0.1 \text{ cm}} \right). \quad (11.23)$$

- [52] M. E. Peskin and D. V. Schroeder, *An Introduction to Quantum Field Theory*, Perseus, Cambridge, MA (1995).
- [53] D. B. Newell et al. (CODATA), Metrologia **55** (2018) L13.
- [54] A. Ceccucci, Z. Ligeti, and Y. Sakai, *12. CKM Quark-Mixing Matrix*, pg. 262 in Ref. [7].

- [55] Z. Fodor, C. Hoelbig, S. Krieg et al., *Up and Down Quark Masses and Corrections to Dashen’s Theorem from Lattice QCD and Quenched QED*, Phys. Rev. Lett. **117** (2016) 082001.
- [56] T. Albahri, A. Anastasi, K. Badgley, S. Baessler, I. Bailey et al. (Muon $g - 2$ Collaboration), *Beam dynamics corrections to the Run-1 measurement of the muon anomalous magnetic moment at Fermilab*, Phys. Rev. Accel. Beams **24** (2021) 044002.
- [57] T. Albahri, A. Anastasi, A. Anisenkov, K. Badgley, S. Baessler et al. (Muon $g - 2$ Collaboration), *Measurement of the anomalous precession frequency of the muon in the Fermilab Muon $g - 2$ Experiment*, Phys. Rev. D **103** (2021) 072002 .
- [58] R. P. Feynman, *Photon-Hadron Interactions*, Addison-Wesley, Redwood City, CA (1972), pgs. 82–85 introduce the vector meson coupling strengths

$$g_V = \alpha \sqrt{4\pi m_V / (3\Gamma_V^{ee})}$$

for $V = \rho, \omega$ and pgs. 96–97 express the pion amplitude ratio

$$g_{\pi\rho\omega}/g_{\pi\gamma\gamma} = g_\rho g_\omega / (4\pi e^2)$$

in terms of these couplings and the electric charge e . Note that $e^2 = \alpha \approx 1/137$ in Feynman’s conventions.

- [59] F. Ambrosino et al. (KLOE Collaboration), *Measurement of the DAΦNE luminosity with the KLOE detector using large angle Bhabha scattering*, Eur. Phys. J. C **47** (2006) 589.
- [60] D. P. Fernandez, Y. Mulev, A. R. Goodwin and J. M. H. Levelt Sengers, *Database for the Static Dielectric Constant of Water and Steam*, J. Phys. Chem. Ref. Data **24** (1995) 33, Table 2 gives the static dielectric constant $\epsilon = 78.43 \pm 0.10$ for liquid water at room temperature $T = 298.14$ K and atmospheric pressure $P_a = 10^5$ Pa by averaging over published measurements of the dielectric response at frequencies ranging from 100 Hz to 40 GHz. The quoted uncertainty is the population standard deviation of these measurements about their average value.
- [61] V. V. Flambaum, D. B. Leinweber, A. W. Thomas, and R. D. Young, *Limits on variations of the quark masses, QCD scale, and fine structure constant*, Phys. Rev. D **69** (2004) 115006. Section III gives $\Delta\nu_{\text{Cs}}/\nu_{\text{Cs}} = 2.83 \Delta\alpha/\alpha$ for the sensitivity of the cesium-133 microwave clock frequency to the electromagnetic fine-structure constant. Combining with the sensitivity $k_\alpha = -2.59$ of the line ratio $\nu_{\text{Yb}}/\nu_{\text{Cs}}$ [36], we obtain the ytterbium-171 optical lattice clock sensitivity $\Delta\nu_{\text{Yb}}/\nu_{\text{Yb}} = (2.83 - 2.59) \Delta\alpha/\alpha = 0.24 \Delta\alpha/\alpha$.
- [62] R. Cardman and G. Raithel, *Driving alkali Rydberg transitions with a phase-modulated optical lattice*, Phys. Rev. Lett. **131** (2023) 023201.
- [63] R. H. Dicke, *The Measurement of Thermal Radiation at Microwave Frequencies*, Rev. Sci. Instrum. **17** (1946) 268.
- [64] C. Bartram et al., (ADMX Collaboration), *Search for “Invisible” Axion Dark Matter in the 3.3 – 4.2 μeV Mass Range*, Phys. Rev. Lett. **127** (2021) 261803.
- [65] K. Ehret, M. Frede, S. Ghazaryan, M. Hildebrandt, E.-A. Knabbe, D. Kracht, A. Lindner, J. List, T. Meier, N. Meyer, D. Notz, J. Redondo, A. Ringwald, G. Wiedemann and B. Willke (ALPS Collaboration), *Resonant laser power build-up in ALPS experiment*, Nucl. Instrum. Meth. A **612** (2009) 83.